Role for the actomyosin complex in regulated exocytosis revealed by intravital microscopy

Andrius Masedunskas[a,b], Monika Sramkova[a], Laura Parente[a], Katiuchia Uzzun Sales[c], Panomwat Amornphimoltham[a], Thomas H. Bugge[c], and Roberto Weigert[a,1]

[a]Intracellular Membrane Trafficking Unit and [c]Proteases and Tissue Remodeling Section, Oral and Pharyngeal Cancer Branch, National Institute of Dental and Craniofacial Research, National Institutes of Health, Bethesda, MD 20892-4340; and [b]Department of Biology, University of North Carolina, Chapel Hill, NC 27514

Edited* by Jennifer Lippincott-Schwartz, National Institutes of Health, Bethesda, MD, and approved July 11, 2011 (received for review November 9, 2010)

The regulation and the dynamics of membrane trafficking events have been studied primarily in in vitro models that often do not fully reflect the functional complexity found in a living multicellular organism. Here we used intravital microscopy in the salivary glands of live rodents to investigate regulated exocytosis, a fundamental process in all of the secretory organs. We found that β-adrenergic stimulation elicits exocytosis of large secretory granules, which gradually collapse with the apical plasma membrane without any evidence of compound exocytosis, as was previously described. Furthermore, we show that the driving force required to complete the collapse of the granules is provided by the recruitment of F-actin and nonmuscle myosin II on the granule membranes that is triggered upon fusion with the plasma membrane. Our results provide information on the machinery controlling regulated secretion and show that intravital microscopy provides unique opportunities to address fundamental questions in cell biology under physiological conditions.

in vivo imaging | cytoskeleton

Regulated exocytosis is a key cellular process in which molecules destined for secretion are packaged into vesicles that constitutively bud from the trans-Golgi network and, upon receiving the appropriate stimuli, fuse with the plasma membrane (PM), releasing their content into the extracellular space (1–4). One of the experimental models that has been extensively used to study the regulated exocytosis is the acinar cells of the salivary glands (SGs) in which the large SCGs, upon stimulation of the appropriate G protein-coupled receptors, fuse with the apical plasma membrane (APM), where they release their contents into a network of canaliculi and ducts (5–7). In SGs, three fundamental questions need to be addressed: (*i*) what stimulus triggers exocytosis of the large SCGs? (*ii*) what is the modality of fusion of SCGs to the APM? and (*iii*) what is the role of the actin cytoskeleton in this process? These issues have been studied extensively in vivo, either by measuring the levels of secreted proteins or by electron microscopy, and both in vitro and ex vivo by using light microscopy. Although these approaches have provided ground-breaking information on several aspects of regulated secretion, they show some limitations. Indeed, the former provides an indirect estimate of the exocytic events, whereas the latter relies on models that do not fully reproduce the complex structural and functional tissue organization found in live animals. Moreover, using isolated acinar preparations, several groups have reported a wide spectrum of contradictory findings. For example, in vivo and ex vivo studies suggest that in parotid and submandibular SGs, the release of secretory proteins is primarily controlled by the β-adrenergic receptor (7, 8). However, other studies showed that the muscarinic receptor can also stimulate exocytosis and play a synergistic role in the β-adrenergic–mediated release of the SCGs (9–11). Furthermore, in secretory cells, SCGs have been proposed to fuse with the PM by one of three different modalities: complete fusion events, kiss-and-run events, and compound exocytosis (4, 12, 13). In explanted SG slices and in acinar preparations from other exocrine tissues, both complete fusion events and compound exocytosis have been observed under different experimental conditions by using either differential interference contrast microscopy (9–11) or two-photon microscopy (4, 11, 13–17). Finally, the role of actin during exocytosis has been extensively investigated, and various models have been proposed. Indeed, actin has been suggested to (*i*) act as a barrier at the APM to limit the fusion of the SCGs, (*ii*) hold SCGs at the APM, (*iii*) direct SCGs to the fusion site, (*iv*) facilitate SCG fusion with the PM, (*v*) control compound exocytosis, and (*vi*) regulate compensatory endocytosis (4, 18–24). Although it is possible that actin is involved in all these processes at the same time, one alternative is that different results reflect the various experimental systems and tools used.

To overcome these issues, we set up an experimental system aimed at imaging and tracking large SCGs in live animals, avoiding those procedures used to isolate and maintain acinar preparations that may impact the experimental outcome (mechanical stress, enzymatic digestion, choice of the appropriate culture media, and proper level of oxygenation). Our approach used confocal intravital microscopy (IVM) as the imaging technique and the submandibular SGs of live rodents, a model organ that we have previously used to study membrane trafficking under physiological conditions (25–27).

In this study, we focus on the dynamics and the machinery regulating the fate of the SCGs after their fusion with the APM. To this aim, we used a combination of transgenic mice and gene transfection into the SGs of live rats, which enabled us to visualize the SCGs, their limiting membranes, their content, and the actin cytoskeleton. Here, we show that exocytosis of the SCGs in the SGs in vivo is elicited exclusively by the β-adrenergic receptor and not the muscarinic receptor. Furthermore, we determine that after fusion with the APM, SCGs completely collapse without any evidence of compound exocytosis. Finally, upon fusion with the APM, F-actin and nonmuscle myosin II are recruited onto the surface of the SCGs, where they provide a scaffold that facilitates the collapse with the APM and prevents the homotypic fusion of the SCGs. These results show that IVM provides the opportunity to study exocytosis in living animals and the dynamics of various cellular processes under physiological conditions.

Results

Imaging the Secretory Granules in the Salivary Glands in Live Animals. In SGs, proteins are secreted at the APM primarily through the

Author contributions: A.M., T.H.B., and R.W. designed research; A.M., M.S., L.P., K.U.S., and P.A. performed research; A.M. and R.W. analyzed data; and A.M. and R.W. wrote the paper.

The authors declare no conflict of interest.

*This Direct Submission article had a prearranged editor.

[1]To whom correspondence should be addressed. E-mail: weigertr@mail.nih.gov.

This article contains supporting information online at www.pnas.org/lookup/suppl/doi:10.1073/pnas.1016778108/-/DCSupplemental.

regulated exocytosis of large SCGs (7). As a model to image the dynamics of these vesicles, we used transgenic mice ubiquitously expressing a soluble form of the green fluorescent protein (GFP) (28). By using intravital two-photon microscopy, we observed that, in the acinar cells of the SGs and the other exocrine glands tested, cytoplasmic GFP was excluded from large vesicles (Figs. S1 and S2). To better resolve these vesicles, we used confocal microscopy, which allows us to control the thickness of the optical slices, providing a higher resolution compared with two-photon microscopy (Fig. S1) (29). On the basis of their size (1–1.5 μm in diameter), behavior (see below), and lack of overlap with markers for other large intracellular organelles, these vesicles were identified as SCGs (Fig. S2). By performing a z-scan of the SGs, we determined the optimal imaging depth to be between approximately 10 and 15 μm below the surface of the glands (Fig. 1*A* and Fig. S3). At this depth, the first layers of acini were optically sectioned in the middle (Fig. S3) where both SCGs (Fig.1*A*, arrowheads) and acinar canaliculi (Fig. 1*A*, arrow) are clearly visible. Indeed, GFP highlighted the APM as identified by the enrichment in cortical F-actin (Fig. 1*B*, *Inset*, and Movie S1). Although we have not established the reason for this enrichment, we speculated that GFP may bind to some of the components of the actin cytoskeleton in a nonspecific fashion.

Regulation of Fusion of Secretory Granules in the Salivary Glands of Live Animals. Because there are conflicting data generated in in vitro and ex vivo systems about the role of β-adrenergic and muscarinic receptors in SGs, we sought to determine which stimulus elicits exocytosis of the SCGs in vivo. Exocytosis was assayed by estimating the reduction in the number of large SCGs after agonist stimulation, as shown by others (8, 11). To this aim, we injected isoproterenol (Iso, a β-adrenergic agonist) and imaged the SCGs by time-lapse confocal microscopy (Fig. 1*C*, *Left*). Thirty minutes after the injection of Iso, we observed an 80% reduction in the number of SCGs and a significant expansion of the acinar canaliculi (Fig. 1*C*, *Right* and *Insets*). The reduction in the number of SCGs was uniformly observed throughout the acini (Movie S2), confirming that SCGs underwent exocytosis. Although our experimental setup did not allow directly imaging the fusion step (i.e., the mixing of the membrane bilayer), this assay provided an indirect estimate of the fusion events of the SCGs with the APM. The maximal rate of degranulation was elicited when between 0.1–0.5 mg/kg of Iso was injected (Fig. 1*D*) and occurred after 2–5 min from the injection. Higher doses of Iso (>0.5 mg/kg) induced the rapid formation of large vacuoles (Fig. S4), which most likely represent a nonphysiological process (30). The same response was also observed in the parotid glands and in the SGs of live rats, and neither the externalization of the glands nor the GFP expression had any effect on the regulation or the rate of degranulation (Fig. S4). Injections of carbachol (Carb, a muscarinic agonist), even at doses comparable to those used in ex vivo explants, did not stimulate any degranulation in contrast to previously reported data (Fig. 1*E*; Fig. S4; Movie S3). However, Carb showed a biological activity because it induced fluid secretion as expected (Fig. S5) (9–11, 31, 32). Finally, coinjection of Iso and Carb did not result in any significant increase in the rate of degranulation (Fig. 1*E* and Fig. S5).

After Fusion with the Apical Plasma Membrane, the Secretory Granules Collapse in a Single Step. Next, we imaged the dynamics of the SCGs at the APM. The scanning speed was increased to 0.2–0.6 s/frame to visualize the large SCGs, which undergo exocytosis in a slow fashion (several seconds up to minutes) (3, 4). Upon injection of Iso, most of the cytoplasmic SCGs increased their motility, whereas those closer to the APM did not. This subpopulation of SCGs exhibited a two- to threefold increase in the GFP fluorescence surrounding it (Movies S4 and S5), which correlated with the recruitment of F-actin (Fig. 2*A*). Notably,

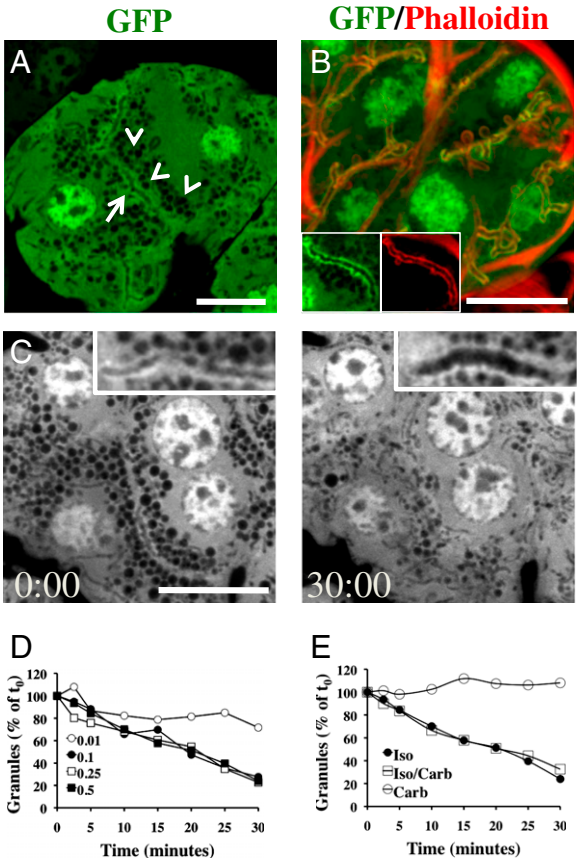

Fig. 1. A transgenic mouse model for dynamic imaging of the SCGs the APM in vivo. The submandibular SGs of anesthetized GFP mice were imaged in situ by IVM (*A* and *C*) or excised and labeled with TRITC–phalloidin to reveal the actin cytoskeleton (*B*). (*A*) Cytoplasmic GFP (green) is excluded from the SCGs (arrowheads) and enriched at the APM (arrow). (*B*) The APM is enriched in GFP (green) and actin as revealed by counterstaining with TRITC–phalloidin (red). (*Insets*) High magnification of a canaliculus. (*C*) The anesthetized GFP mice received a s.c. injection of 0.5 mg/kg Iso, and the SGs were imaged by time-lapse confocal microscopy. Acinus imaged at the moment of Iso injection (*Left*) or after 30 min (*Right*) (Movies S2 and S3). High magnification of the canaliculi (*Insets*). (Scale bars, 10 μm.) (*D* and *E*) Quantitation of the degranulation of the SCGs. Data shown are measurements from a single acinus. The experiments were performed three times with similar results. (*D*) Exocytosis in response to various doses of Iso: 0.01 mg/kg (○), 0.1 mg/kg (●), 0.25 mg/kg (□), and 0.5 mg/kg (■). (*E*) Exocytosis in response to muscarinic or adrenergic stimulation: 0.01 mg/kg Carb (○), 0.1 mg/kg Iso (●) or both (□).

these SCGs decreased in size slowly (40–60 s) and gradually collapsed into the APM (Fig. 2*B*, arrows, and *C*, and Movie S6), suggesting that exocytosis of SCGs was imaged. This idea is further supported by the fact that these events were observed only when degranulation was stimulated by Iso (Movie S3). Previous studies in acinar preparations of explanted exocrine glands showed that this process occurs through compound exocytosis rather than through single fusion events (4, 11, 33). Compound exocytosis has been defined as the process by which large SCGs fuse with SCGs that are already connected with the APM, generating strings of three to four interconnected granules (13). These strings, which have been reported to be stable for more than 20 s, should have been detectable under the imaging conditions used in this study (17, 34). However, we cannot exclude that, due to the thin optical slices used to image the SCGs in the GFP mice, some of the interconnections between the fusing SCGs might have been missed. To clarify this, we used two alternative approaches. First, we slowly infused a fluorescently labeled dex-

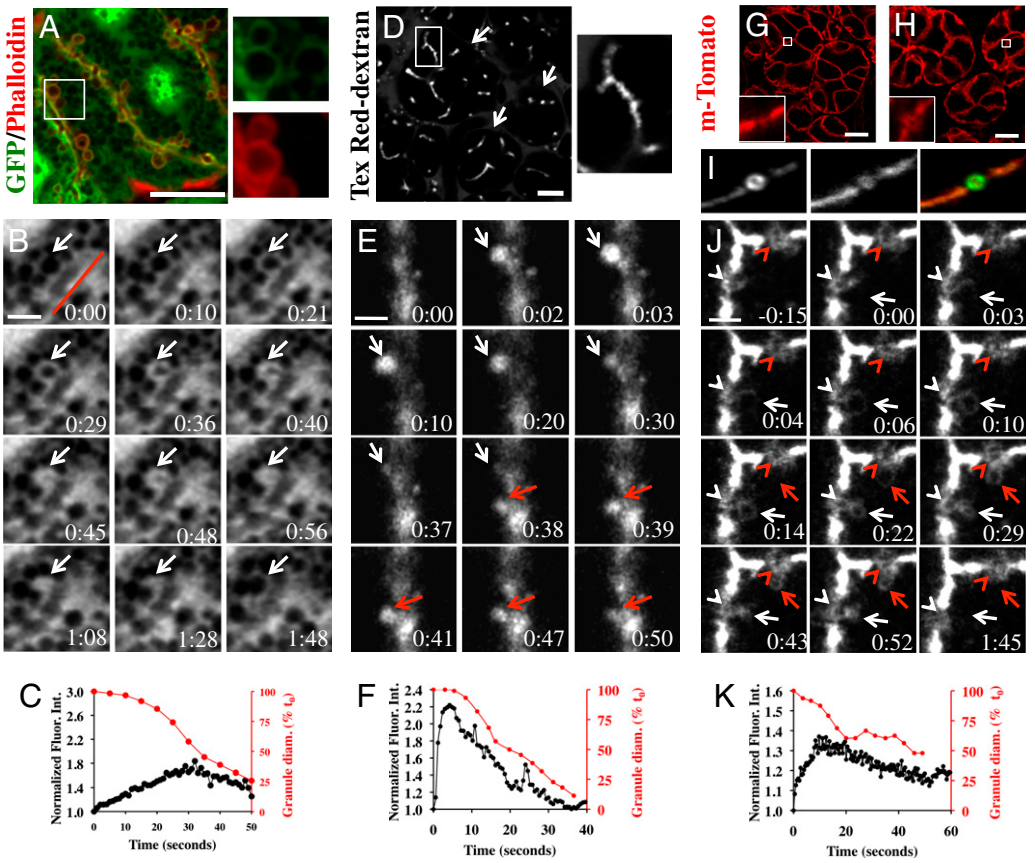

Fig. 2. SCGs completely collapse after fusion with the APM. (*A*) SCGs close to the APM are enriched in GFP. Anesthetized GFP mice were injected s.c. with 0.1 mg/kg Iso, and after 10 min, excised and labeled with TRITC–phalloidin. Granules close to the APM are coated with actin (red) and also enriched in GFP (green). (Scale bar, 10 μm.) (*B*) Time series of a single granule (white arrows) fusing with the APM (red line) (red arrowheads in Movie S6). (Scale bar, 3 μm.) (*C*) Quantitation of both the GFP fluorescence intensity around a SCG (black circles) and its diameter (red circles) during Iso-stimulated exocytosis. Data shown are from a single event. Five events per animal were measured in two independent experiments. (*D–F*) Texas Red–dextran (10 kDa) was infused by gravity into the salivary ducts of a live anesthetized rat. The SGs were exposed and imaged by confocal microscopy. (*D*) Canaliculi are highlighted in the acini (arrows). (*Inset*) High magnification of a canaliculus. (Scale bar, 10 μm.) (*E* and *F*) Iso (0.1 mg/kg) was injected s.c. (*E*) Time-lapse sequence. When the fusion pore opens, dextran enters two SCGs (white and red arrows), enabling their visualization. (Scale bar, 3 μm.) (Movie S7). (*F*) The fluorescence intensity of the dextran inside the granule shown in *E* (white arrows) was measured (black circles) and correlated with its diameter (red circles) as described in *Materials and Methods*. Data shown are from a single event. Four to five events per animal were measured in two independent experiments. (*G–J*) Anesthetized m-Tomato mice were left untreated (*G* and *I*) or injected with Iso (*H*, *J*, and *K*). The SMGs were imaged in situ (*G*, *H*, and *J*) or labeled with TRITC–phalloidin (*I*). Acinar canaliculi in cross-section [*G*, *H* (*Inset*), and *I*]. (*J*) Time series of the collapse of two SCGs revealed by the diffusion of the m-Tomato from the APM (white and red arrows). Note the expansion of the canaliculi (white and red arrowheads). (Scale bar, 3 μm.) (Movie S9). (*K*) The fluorescence intensity of the m-Tomato at the surface of a granule (black circles) and its diameter (red circles) were measured as described in *Materials and Methods*. Data shown are measurements of a single event. A total of 6–10 events per animal were recorded in three independent experiments.

tran into the ductal system of a live rat (Fig. 2*D*) (27). This approach mimics the bathing of the explanted glands in small fluorescent probes that has been used to investigate exocytosis in ex vivo models (11, 13, 14, 16, 17, 35). For this set of experiments, we used larger optical sections (1–1.2 μm, Fig. S1) closely matching those achieved by two-photon microscopy experiments that have been successfully used to image compound exocytosis (15). Upon injection of Iso, the dye rapidly filled large vesicular structures, which later gradually collapsed with the APM (Fig. 2 *E* and *F* and Movie S7). On the basis of their size (1–1.5 μm in diameter), we argued that these structures represent SCGs, which have fused with the APM and have been filled with fluorescent dextran upon the opening of the fusion pore. This was confirmed by performing the same experiment in the mouse expressing soluble GFP, where the SCGs are visible (Fig. S6). Under these conditions, we did not observe any evidence of compound exocytosis. Second, we used a transgenic mouse ubiquitously expressing a membrane-targeted peptide fused with the fluorescent protein tdTomato (m-Tomato mice) (36). This reporter localized both at the apical and the basolateral PM but not in the SCGs (Fig. 2*G*). The apical canaliculi were easily identified on the basis of their characteristic F-actin coat and morphology (Fig. 2*I* and Movie S8). In this model, we expected the m-Tomato to diffuse into the SCGs upon fusion with the APM, thus enabling us to track their fate. Also in this case, the optical section was increased to 1–1.2 μm to optimize the detection of the SCGs and the APM (Fig. S1). After injection of Iso, m-Tomato localized onto large circular structures (1–1.5 μm in diameter), and the acinar canaliculi appeared enlarged as shown for the GFP mice (Fig. 2*H*). Time-lapse imaging showed that, upon injection of Iso, the m-Tomato circular profiles completely collapsed at a rate (40–60 s) similar to that observed for the SCGs in the GFP mice (Fig. 2*J* and Movie S9). Fusing SCGs clustered around the expanded canaliculi, but compound exocytosis was not observed (Fig. 2*J*). These vesicles represented the fused SCGs as shown by crossing the m-Tomato mice with the GFP mice (Fig. S6).

Overall, our data support the idea that large SCGs in the SGs in vivo fuse at the PM and release their contents in the extra-

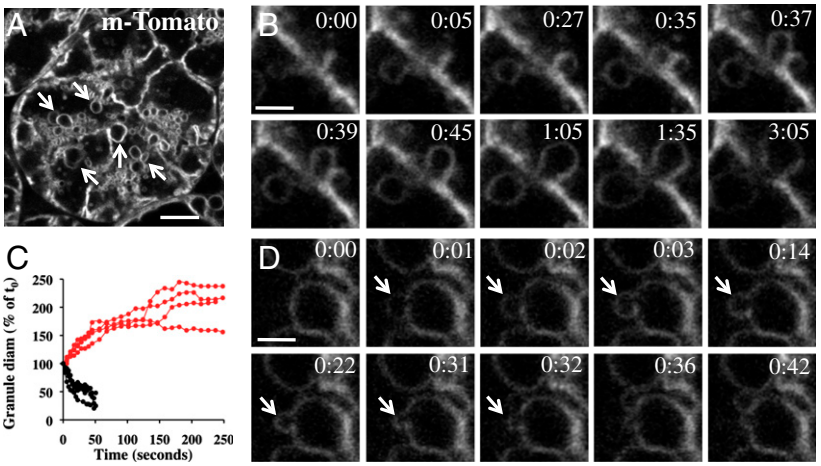

Fig. 3. Role of the actin cytoskeleton in facilitating the collapse of the SCGs. (*A–D*) The SGs of the m-Tomato mice were exposed to 10 μM CD, and after 20 min the animals received a s.c.injection of 0.1 mg/kg Iso. (*A*) The SGs were exposed and imaged in situ. Large vacuoles were observed in the cytoplasm of the acinar cells (arrows). (Scale bar, 10 μm.) (*B–D*) Time-lapse sequence of SCGs after fusion with the APM, 2 min (*B*) or 10 min (*D*) after the injection of Iso. (*B*) The SCGs fuse with the APM, do not collapse, and form large vacuoles. (Scale bar, 3 μm.) (Movie S12). (*C*) Quantitation of the diameter of the vacuoles that fail to collapse after fusion with the APM in the presence of CD (red circles) and of the granules that fuse under control conditions (black circles). Data shown are from four granules in the same acinus. A total of 10–15 granules were analyzed in two independent experiments. (*D*) A SCG fuses with a large vacuole and rapidly collapses (arrows) (Movie S14).

cellular space in a single event, which leads to the controlled collapse of the granules into the APM. Although we have not observed any compound exocytosis of large SCGs, due to the spatial and temporal limitations of our experimental system, we cannot rule out that smaller vesicular structures (between 50 and 100 nm) fuse with the SCGs during the collapse.

F-Actin Is Recruited on the Secretory Granules After Membrane Fusion with the Apical Plasma Membrane and Is Required to Drive Their Collapse to Completion. We observed that the size of the SCGs did not change for the first 5–10 s after fusion with the APM (Fig. 2 *C*, *F*, and *K*, red circles). During this time the m-Tomato diffused into the SCGs with what appeared to be a slow rate. Interestingly, the fusion pore opened in parallel with the diffusion of the m-Tomato, as shown by infusing fluorescently labeled dextran into the ductal system of the m-Tomato mouse and stimulating exocytosis with Iso (Fig. S7). After the intensity of the m-Tomato fluorescence reached a maximum, the granules sharply decreased in size (Fig. 2*K*, black circles). We hypothesized that this lag time was due to the recruitment of the machinery regulating the collapse of the granules. Because F-actin coated the granules close to the APM (Fig. 2*A*), we investigated whether it could play a role in facilitating this step. To this aim, we labeled the SGs of the m-Tomato mice for F-actin after stimulation with Iso. We observed that 100% of the F-actin–coated granules (481 granules scored; $n = 3$) were labeled with the m-Tomato, whereas 2.8 ± 1.8% (average ± SEM, $n = 3$) of the m-Tomato-labeled granules were not labeled with F-actin (Fig. S8). This finding suggested that F-actin was recruited onto the SCGs only after membrane fusion had occurred. Next, we analyzed the dynamics of F-actin recruitment onto the SCGs by transfecting the acini of live rats with GFP–lifeact, a probe that dynamically labels F-actin without compromising its function (37). We have previously shown that the acini in the SGs can be selectively transfected with fluorescently tagged proteins (27). As expected, in acinar cells, GFP–lifeact showed a distribution comparable to that of F-actin. In control conditions, GFP–lifeact was localized at the PM and enriched at the apical pole (Fig. S8). Upon stimulation with Iso, GFP–lifeact was recruited onto the SCGs and then progressively released during their collapse (Fig. S8 and Movie S10). To analyze the kinetics of F-actin recruitment with respect to the dynamics of the SCGs, we cotransfected red fluorescent protein–lifeact (RFP–lifeact) with GFP–farnesyl, a marker for the PM (38) that behaves similarly to the m-Tomato both in resting conditions and under stimulation (Fig. S8). F-actin was recruited onto the SCGs after a short lag time coinciding with the initial diffusion of membranes from the canaliculi, suggesting that some of the factors controlling the nucleation or the assembly of F-actin might come from the APM (Fig. S8). This finding also suggests that F-actin assembly occurs after the opening of the fusion pore and most likely does not play any role in this process. Finally, we pharmacologically disrupted the actin cytoskeleton in live animals by using cytochalasin D (CD) (Fig. 3) or latrunculin A (Fig. S9). In resting conditions, no exocytic events were observed, although some small vesicular structures of unknown origin were observed in close proximity to the PM (Movie S11). Upon injection of Iso, SCGs fused with the APM at the same rate described above, but failed to collapse (Fig. 3 *A*, arrows, and *B*, and Movie S12) and increased in size, forming large vacuoles two- to threefold larger than the normal granules, as shown by measuring their diameter over time (Fig. 3*C*, red circles). These vacuoles were generated by the SCGs fusing with the APM, and not as a result of interfering with endocytic events, as shown by disrupting the actin cytoskeleton in GFP mice (Fig. S9). Furthermore, we observed that the remaining SCGs fused and rapidly collapsed with the vacuoles in a process reminiscent of compound exocytosis (Fig. 3*D* and Movie S13). Latrunculin A treatment produced similar results (Fig. S9). These observations suggest that F-actin may play a role in controlling the collapse of the granules and in preventing their homotypic fusion that was not observed under control conditions. Moreover, F-actin may provide a scaffold preventing the expansion of the SCGs that may be driven by the hydrostatic pressure generated by the fluid secretion that we observed during the exocytic process (Fig. S10 and Movie S14).

Finally, we observed that 5–10 min after stimulation with Iso the total amount of secreted protein was inhibited by almost 50% (Fig. S9). Because we ruled out that the impairment of the actin cytoskeleton affected the opening of the fusion pore (Fig. S9), this inhibition may be explained by the fact that the failure of the first SCGs to collapse prevented the discharge of the cargo proteins into the canaliculi. However, after 30 min, all of the SCGs completely fused with the large vacuoles (Fig. S9), and the level of the secreted protein was comparable to that measured in control conditions. This suggests that the cargo proteins retained in the vacuoles were released into the canaliculi, possibly facilitated by the fluid secretion accompanying exocytosis.

Myosin IIa and IIb Are Recruited onto the Granules and Their Motor Activity Facilitates the Collapse of the Secretory Granules. The role of F-actin in facilitating the collapse of the SCGs may be linked to the assembly of an actomyosin complex, as described for the contractile ring during cytokinesis (39, 40). Indeed, nonmuscle myosin IIa has been previously implicated in the regulation of the opening and the closing of the fusion pore during regulated secretion (14, 15, 41). We determined that, under resting conditions, both myosin IIa and IIb localized in the cytoplasm and at the APM in the SGs (Fig. 4 *A* and *C*), whereas upon stimulation with Iso, both isoforms were recruited onto the surface of the

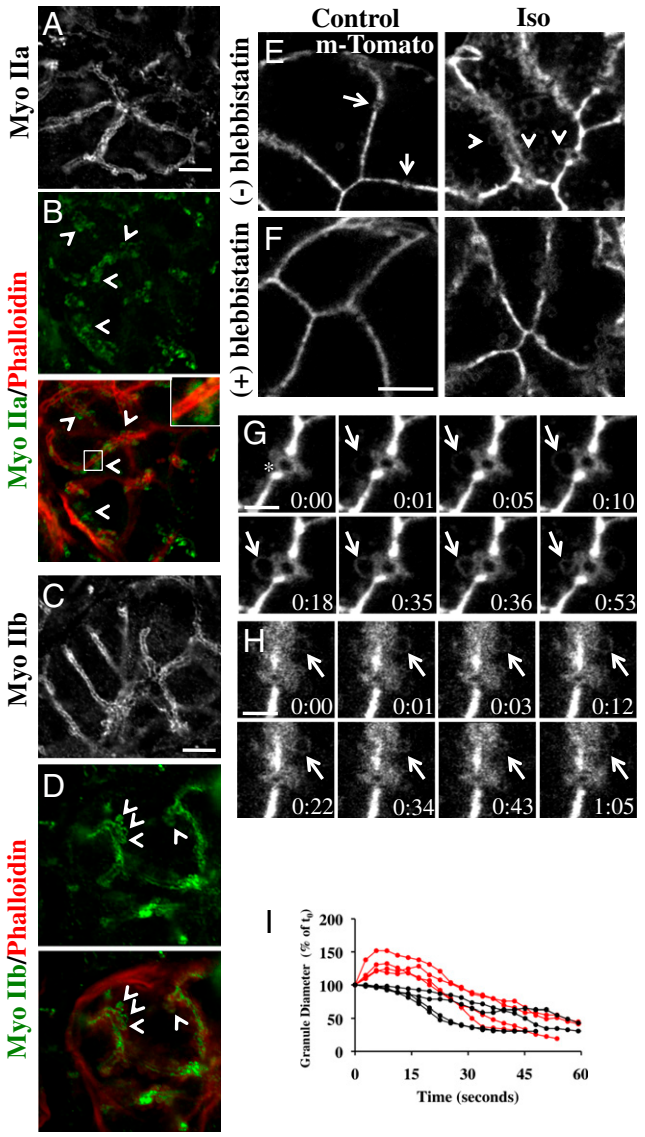

Fig. 4. Role of myosin IIa and IIb in the collapse of the secretory granules. (*A–D*) Friend Virus B-Type (FVB) mice were left untreated (*A* and *C*) or injected with 0.1 mg/kg Iso (*B* and *D*). SGs were excised and labeled for endogenous nonmuscle myosin IIa (*A* and *B*) and IIb (*C* and *D*) and actin (*B* and *C*) as described in *Materials and Methods*. Upon stimulation with Iso, both myosin types are localized in SCGs at the APM (arrowheads). (*Inset* in *B*) An SCG at the APM. (Scale bars, 10 μm.) (*E–H*) The SGs of m-Tomato mice were exposed and incubated with 50 μM of either (−)Bleb (*E* and *G*) or (+) Bleb (*F* and *H*). After 20 min, the SGs were imaged (*E* and *F*, *Left* panels). In the presence of (−)Bleb, the acinar canaliculi expanded (arrows). The mice were then injected s.c. with 0.1 mg/kg Iso and imaged in time-lapse mode (*E* and *F*, *Right* panels, and *G* and *H*). (*E* and *F*) Snapshots taken 10 min after the Iso injection. Large granules appeared at the APM (arrowheads). (Scale bar in *F*, 10 μm.) (*G* and *H*) Time-lapse sequence of SCGs fusing with APM (Movies S15 and S16). Expanded canaliculus (asterisk). (Scale bars, 3 μm.) (*I*) Quantitation of the diameter of the SCGs after fusion with the APM in the presence of (−)Bleb (red circles) or (+)Bleb (black circles). Data shown are from four granules in the same acinus. A total of 15–20 granules were analyzed in two independent experiments.

fusing granules (Fig. 4 *B* and *D*, arrowheads). To determine whether these myosins were involved in SCG exocytosis, we pharmacologically blocked their motor activity by using (−) blebbistatin (Bleb), a specific inhibitor of the myosin II ATPase (42). In animals treated with (−)Bleb, we observed the appearance of few intracellular vesicles of unknown origin and the enlargement of the acinar canaliculi (Fig. 4*E*, arrows). Upon stimulation with Iso, although the onset of the fusion events was not affected, the acinar canaliculi further expanded and granules of larger size appeared at the APM (Fig. 4*E*, arrowheads). Time-lapse sequences showed that a significant proportion of SCGs fused with the APM and abruptly increased in size, as observed when the actin cytoskeleton was disrupted (Fig. 4 *G* and *I* and Movie S15). However, under these conditions, SCGs collapsed with the APM, and only a small population collapsed at a slower rate compared with the inactive stereoisomer (+)Bleb (Fig. 4 *H* and *I* and Movie S16). These data suggest that myosin IIa and IIb are part of the machinery that regulates the collapse of the granules after fusion with the APM.

Discussion

Here we have shown that IVM enables the imaging of dynamic subcellular processes in small rodents. Specifically, here we have investigated the exocytosis of large SCGs in SGs in vivo, showing that this process is regulated in a different fashion than what was previously reported in ex vivo systems and revealing aspects that were not previously appreciated (9–11, 24).

First, we have found that the β-adrenergic and not the muscarinic receptors elicit the fusion of the SCGs with the APM and that this process occurs in SGs in vivo through single fusion events and not through compound exocytosis (4, 11). The reason(s) for the discrepancy between the data derived from explanted organs or acinar preparations and the animal model are difficult to determine. One possible explanation is that the damages derived from the mechanical or enzymatic procedures used to prepare the tissues may activate or alter various signaling pathways, favoring the docking of the granules at the APM and their sensitivity to Ca^{2+} signaling, as shown for lysosomal secretion during membrane repair (43). Moreover, these procedures may disrupt the actin cytoskeleton, resulting in the fusion between the granules at the APM, reminiscent of compound exocytosis (11).

Furthermore, we have determined that F-actin serves many functions during stimulated secretion in the SGs. First, we have shown that F-actin provides a scaffold counteracting hydrostatic imbalances that might interfere with the dynamics of the granules. This role is most likely restricted to the exocrine glands where regulated exocytosis at the APM is accompanied by fluid secretion. Notably, such a role for F-actin has not been described in ex vivo systems where the hydrostatic pressure does not build up due to the lack of an intact ductal system. Second, we have shown that F-actin prevents the fusion between the SCGs accumulated in the apical area and those fused with the APM. In secretory systems in which the collapse of the SCGs is a slow process, the fused granules may have acquired components of the APM, which makes them more susceptible to fusion with other SCGs (44). To prevent these fusion events, F-actin could be recruited onto the SCGs, performing a "barrier" function similar to what has been proposed for the F-actin at the APM (18, 23). Finally, we have shown that F-actin is required to drive the collapse of the SCGs to the APM (Figs. S11 and S12). Our data suggests that F-actin serves as a platform to recruit the actin motors myosin IIa and IIb to form a contractile scaffold that generates the force required for the collapse of the granules (Fig. S12). The impairment of the assembly of F-actin around the fused SCGs leads to a substantial increase in their size and a complete block of their collapse. On the other hand, the inhibition of the motor activity of myosin II results in a sharp increase in the size of all of the fused SCGs and in the delay of the kinetics of the collapse but in only a small subpopulation of the SCGs. The fact that (−)Bleb did not completely block the collapse of the granules might be due to a partial inhibition of the myosin activity, and, unfortunately, higher concentrations of (−)Bleb could not be used because they induce nonspecific effects on the cell membranes. Two other possibilities are that either other molecules are involved in this

process (e.g., another myosin) or that, when myosin II activity is impaired, the collapse of the SCGs is regulated by a different mechanism. Moreover, because (−)Bleb inhibits the activity of both myosin IIa and IIb, we could not assess whether the mysosins perform different functions during SCG exocytosis in SGs as described in other systems (14, 15, 45).

Overall, our data show that the dynamics of exocytosis of large SCGs can be studied in live animals by IVM at the level of the single exocytic event. We have shown that, in the SGs, granules undergo fusion at the APM and slowly collapse, releasing their contents in a process that requires the involvement of the actin cytoskeleton.

It is important to emphasize that our approach shows some limitations. Although we have successfully analyzed the dynamics of large SCGs (this study) and endosomal structure (27–29), it will probably be more difficult to study smaller structures such as 50-nm synaptic vesicles that exocytose in a few milliseconds. However, microscopes with faster scanning speed and genetically encoded probes with higher quantum efficiency may soon overcome this current difficulty.

In conclusion, we have shown that IVM is a powerful tool for studying subcellular events in physiological conditions. We envision that this approach could be extended to other exocrine glands such as the pancreas and the lacrimal glands or other secretory organs that are surgically accessible and, more broadly, to address fundamental biological issues in other areas of cell biology.

Materials and Methods

Animals were brought into the laboratory from the vivarium at least 2 d before the experiment, fed chow and water ad libitum, and allowed to acclimate in the new environment to prevent stress-induced secretion that may affect the outcome of the experiments (8). Animals were anesthetized, the SGs were externalized, and the body temperature of the animals was controlled (25). Controlling the appropriate temperature (around 37 °C) is one of the major sources of variability for this kind of experiment. Imaging was performed in the inverted configuration (Fig. S1). The externalized SGs were accommodated on a coverslip mounted on the stage above the objective. The SGs and the body of the animal were immobilized using custom-made holders. Particular care was taken in controlling the blood flow so that it was not significantly reduced as a consequence of excessive pressure applied on the tissue. This can be assessed by visually looking at the flow of the erythrocytes in the vessels close to the acinar structures. All secretogues were injected s.c. into the dorsal side of the animal.

ACKNOWLEDGMENTS. We thank Drs. J. S. Gutkind, J. Donaldson, P. Randazzo, and M. J. Danton for critical reading of the manuscript. This research was supported by the Intramural Research Program of the National Institutes of Health, National Institute of Dental and Craniofacial Research.

1. Burgoyne RD, Morgan A (2003) Secretory granule exocytosis. *Physiol Rev* 83:581–632.
2. De Matteis MA, Luini A (2008) Exiting the Golgi complex. *Nat Rev Mol Cell Biol* 9: 273–284.
3. Sudhof TC (2004) The synaptic vesicle cycle. *Annu Rev Neurosci* 27:509–547.
4. Sokac AM, Bement WM (2006) Kiss-and-coat and compartment mixing: Coupling exocytosis to signal generation and local actin assembly. *Mol Biol Cell* 17:1495–1502.
5. Castle AM, Huang AY, Castle JD (2002) The minor regulated pathway, a rapid component of salivary secretion, may provide docking/fusion sites for granule exocytosis at the apical surface of acinar cells. *J Cell Sci* 115:2963–2973.
6. Castle JD (1998) Protein secretion by rat parotid acinar cells. Pathways and regulation. *Ann N Y Acad Sci* 842:115–124.
7. Gorr SU, Venkatesh SG, Darling DS (2005) Parotid secretory granules: Crossroads of secretory pathways and protein storage. *J Dent Res* 84:500–509.
8. Peter B, Van Waarde MA, Vissink A, 's-Gravenmade EJ, Konings AW (1995) Degranulation of rat salivary glands following treatment with receptor-selective agonists. *Clin Exp Pharmacol Physiol* 22:330–336.
9. Segawa A, Terakawa S, Yamashina S, Hopkins CR (1991) Exocytosis in living salivary glands: Direct visualization by video-enhanced microscopy and confocal laser microscopy. *Eur J Cell Biol* 54:322–330.
10. Segawa A, Riva A (1996) Dynamics of salivary secretion studied by confocal laser and scanning electron microscopy. *Eur J Morphol* 34:215–219.
11. Warner JD, et al. (2008) Visualizing form and function in organotypic slices of the adult mouse parotid gland. *Am J Physiol Gastrointest Liver Physiol* 295:G629–G640.
12. Pickett JA, Edwardson JM (2006) Compound exocytosis: Mechanisms and functional significance. *Traffic* 7:109–116.
13. Kasai H, et al. (2006) Two-photon excitation imaging of exocytosis and endocytosis and determination of their spatial organization. *Adv Drug Deliv Rev* 58:850–877.
14. Larina O, et al. (2007) Dynamic regulation of the large exocytotic fusion pore in pancreatic acinar cells. *Mol Biol Cell* 18:3502–3511.
15. Bhat P, Thorn P (2009) Myosin 2 maintains an open exocytic fusion pore in secretory epithelial cells. *Mol Biol Cell* 20:1795–1803.
16. Thorn P, Parker I (2005) Two phases of zymogen granule lifetime in mouse pancreas: Ghost granules linger after exocytosis of contents. *J Physiol* 563:433–442.
17. Nemoto T, Kojima T, Oshima A, Bito H, Kasai H (2004) Stabilization of exocytosis by dynamic F-actin coating of zymogen granules in pancreatic acini. *J Biol Chem* 279: 37544–37550.
18. Muallem S, Kwiatkowska K, Xu X, Yin HL (1995) Actin filament disassembly is a sufficient final trigger for exocytosis in nonexcitable cells. *J Cell Biol* 128:589–598.
19. Malacombe M, Bader MF, Gasman S (2006) Exocytosis in neuroendocrine cells: New tasks for actin. *Biochim Biophys Acta* 1763:1175–1183.
20. Satoh K, et al. (2009) Phosphorylation of myristoylated alanine-rich C kinase substrate is involved in the cAMP-dependent amylase release in parotid acinar cells. *Am J Physiol Gastrointest Liver Physiol* 296:G1382–G1390.
21. Sankaranarayanan S, Atluri PP, Ryan TA (2003) Actin has a molecular scaffolding, not propulsive, role in presynaptic function. *Nat Neurosci* 6:127–135.
22. Valentijn JA, Valentijn K, Pastore LM, Jamieson JD (2000) Actin coating of secretory granules during regulated exocytosis correlates with the release of rab3D. *Proc Natl Acad Sci USA* 97:1091–1095.
23. Eitzen G (2003) Actin remodeling to facilitate membrane fusion. *Biochim Biophys Acta* 1641:175–181.
24. Nashida T, Yoshie S, Imai A, Shimomura H (2004) Presence of cytoskeleton proteins in parotid glands and their roles during secretion. *Arch Oral Biol* 49:975–982.
25. Masedunskas A, Weigert R (2008) Intravital two-photon microscopy for studying the uptake and trafficking of fluorescently conjugated molecules in live rodents. *Traffic* 9: 1801–1810.
26. Weigert R, Sramkova M, Parente L, Amornphimoltham P, Masedunskas A (2010) Intravital microscopy: A novel tool to study cell biology in living animals. *Histochem Cell Biol* 133:481–491.
27. Sramkova M, Masedunskas A, Parente L, Molinolo A, Weigert R (2009) Expression of plasmid DNA in the salivary gland epithelium: Novel approaches to study dynamic cellular processes in live animals. *Am J Physiol Cell Physiol* 297:C1347–C1357.
28. Hadjantonakis AK, Gertsenstein M, Ikawa M, Okabe M, Nagy A (1998) Generating green fluorescent mice by germline transmission of green fluorescent ES cells. *Mech Dev* 76:79–90.
29. Diaspro A, Shepard CJR (2002) Two-Photon Microscopy: Basic Principles and Architectures. *Confocal and Two-Photon Microscopy. Foundations, Applications, and Advances,* ed Diaspro A (Wiley-Liss, New York).
30. Sheetz JH, Morgan AH, Schneyer CA (1983) Morphological and biochemical changes in the rat parotid gland after compensatory and isoproterenol-induced enlargement. *Arch Oral Biol* 28:441–445.
31. Turner RJ, Sugiya H (2002) Understanding salivary fluid and protein secretion. *Oral Dis* 8:3–11.
32. Wang CC, et al. (2007) VAMP8/endobrevin as a general vesicular SNARE for regulated exocytosis of the exocrine system. *Mol Biol Cell* 18:1056–1063.
33. Kanno T (2004) Compound exocytosis of secretory granules containing salivary chromogranin A in granular duct cells in rat submandibular gland: The last study in collaboration with the late Professor Noboru Yanaihara at Yanaihara Institute. *Regul Pept* 123:3–7.
34. Nemoto T, et al. (2001) Sequential-replenishment mechanism of exocytosis in pancreatic acini. *Nat Cell Biol* 3:253–258.
35. Thorn P, Fogarty KE, Parker I (2004) Zymogen granule exocytosis is characterized by long fusion pore openings and preservation of vesicle lipid identity. *Proc Natl Acad Sci USA* 101:6774–6779.
36. Muzumdar MD, Tasic B, Miyamichi K, Li L, Luo L (2007) A global double-fluorescent Cre reporter mouse. *Genesis* 45:593–605.
37. Riedl J, et al. (2008) Lifeact: A versatile marker to visualize F-actin. *Nat Methods* 5: 605–607.
38. Rocks O, Peyker A, Bastiaens PI (2006) Spatio-temporal segregation of Ras signals: One ship, three anchors, many harbors. *Curr Opin Cell Biol* 18:351–357.
39. Conti MA, Adelstein RS (2008) Nonmuscle myosin II moves in new directions. *J Cell Sci* 121:11–18.
40. Beach JR, Egelhoff TT (2009) Myosin II recruitment during cytokinesis independent of centralspindlin-mediated phosphorylation. *J Biol Chem* 284:27377–27383.
41. Jerdeva GV, et al. (2005) Actin and non-muscle myosin II facilitate apical exocytosis of tear proteins in rabbit lacrimal acinar epithelial cells. *J Cell Sci* 118:4797–4812.
42. Kovács M, Tóth J, Hetényi C, Málnási-Csizmadia A, Sellers JR (2004) Mechanism of blebbistatin inhibition of myosin II. *J Biol Chem* 279:35557–35563.
43. Idone V, et al. (2008) Repair of injured plasma membrane by rapid Ca2+-dependent endocytosis. *J Cell Biol* 180:905–914.
44. Pickett JA, Thorn P, Edwardson JM (2005) The plasma membrane Q-SNARE syntaxin 2 enters the zymogen granule membrane during exocytosis in the pancreatic acinar cell. *J Biol Chem* 280:1506–1511.
45. Togo T, Steinhardt RA (2004) Nonmuscle myosin IIA and IIB have distinct functions in the exocytosis-dependent process of cell membrane repair. *Mol Biol Cell* 15:688–695.